SAND99-2080J

For publication in Tribology Letters

Structure-Dependent Viscoelastic Properties of C_9-Alkanethiol Monolayers

RECEIVED
AUG 18 1999
OSTI

Neal D. Shinn(1), Thomas M. Mayer and Terry A. Michalske

Sandia National Laboratories, Surface and Interface Sciences Department

P. O. Box 5800, Mail Stop 1413, Albuquerque, NM 87185-1413

Abstract

Quartz crystal microbalance techniques and *in situ* spectroscopic ellipsometry are used to probe the structure-dependent intrinsic viscoelastic properties of self-assembled $CH_3(CH_2)_8SH$ alkanethiol monolayers adsorbed from the gas phase onto Au(111)-textured substrates. Physisorbed molecules, mixed chemisorbed-fluid/solid phases and solid-phase domain boundaries make sequentially dominant contributions to the measured energy dissipation in the growing monolayer. Deviations from Langmuir adsorption kinetics reveal a precursor-mediated adsorption channel. These studies reveal the impact of structural heterogeneity in tribological studies of monolayer lubricants.

Key Words:

alkanethiol, self-assembled monolayers, quartz crystal microbalance, viscoelasticity, kinetics, ellipsometry

---

(1) Corresponding author: ndshinn@sandia.gov

1. Introduction:

Self-assembled monolayers (SAMs) alter not only the chemical functionality of a surface but also its physical properties [1]. By selecting appropriate constituent molecules and controlling the growth conditions, SAM-coated material interfaces could be engineered for optimal lubrication, adhesion, or vibration damping characteristics. For this reason, SAMs are attractive candidates as interfacial lubricants in micro-electromechanical systems where traditional lubricants cannot be used. However, recent counter-intuitive discoveries, such as higher friction for hydrocarbon vs. fluorocarbon SAMs [2], demonstrate an inadequate understanding of energy dissipation at monolayer interfaces. Friction experiments can be difficult to interpret unambiguously because they measure the energy dissipation due to *intrinsic* monolayer viscoelastic properties combined with *extrinsic* contributions from probe/monolayer interactions. Separating these intrinsic and extrinsic contributions will allow us to better understand friction and thereby synthesize monolayers with optimal mechanical properties.

We accomplish this by using quartz crystal microbalance (QCM) techniques to inertially shear and simultaneously measure only the *intrinsic* viscoelastic properties of a self assembled nonyl mercaptan [$CH_3(CH_2)_8SH$] monolayer (denoted hereafter as C_9 thiol) on Au(111)-textured electrodes. These molecules form ordered c(4x2) domains of vertically inclined chemisorbed molecules [3-10] shown schematically in Figure 1. The ideal saturation coverage, defined as one monolayer (ML), corresponds to 0.33 molecules per substrate Au atom. Due to the Au(111) c_{3v} symmetry, equivalent domains can co-exist with molecules tilted in one of three azimuths. Scanning tunneling microscopy experiments on single crystal Au(111) substrates show that regions as small as ~100 nm^2 can consist of multiple c(4x2) domains with incommensurate boundaries and inclusions of disordered molecules [11]. Even within one domain, helium diffraction, X-ray diffraction [9, 10] and photoemission experiments [12] indicate a more subtle inhomogeneity with the sulfur head groups of neighboring molecules bonded at inequivalent Au(111) adsorption sites [13]. Not only do conformational disorder and vacancies contribute to monolayer inhomogeneity, but molecular dynamics simulations of our previous QCM experiments showed that these structural defects were necessary to introduce energy dissipation channels [14]. This suggests that monolayer structure is a crucial variable in determining the magnitude of energy dissipation. Understanding how the different aspects of structural inhomogeneity contribute to energy dissipation during dynamic shear is the objective of this work.

2. Experimental:

A viscoelastic monolayer on the QCM electrode surfaces adds a mechanical impedance to the vibrating QCM, which is manifested electrically by a decrease in the resonant frequency (mass loading), and increased resonator impedance (vibrational amplitude damping). Using acoustic theory, these electrical changes can be related to the complex shear modulus ($\mathbf{G}_{SAM}$ = G' + *i* G") for a monolayer of known density and thickness [15-17]. This approach has been used previously to show that the elastic shear modulus (G') for solution-deposited alkanethiol monolayers increases with alkane chain length [14]. However, the shear loss modulus (G") of an ultrathin film is difficult to measure accurately by this method [18]. Instead, we use a high-sensitivity oscillator circuit to measure relative changes in energy dissipation [19].

In the present studies, we measure changes in the energy dissipation as C_9 thiol molecules adsorb from the gas phase and self-assemble on the gold electrodes of commercially available 5MHz QCM crystals (Maxtek) . Clean Au(111)-textured electrode surfaces of <10Å rms roughness (measured by *ex situ* atomic force microscopy) were prepared by *in situ* Au evaporation onto a masked QCM mounted in a high vacuum chamber ($p < 1 \times 10^{-7}$ torr). An electrically isolated chromel alumel thermocouple junction attached to the crystal edge provided temperature feedback to a thermostatically-controlled cooling system, thereby maintaining a constant temperature (±0.1°C) and stable resonant frequency (±0.1 Hz).

C_9 thiol vapor was admitted into the chamber via a calibrated leak valve while continuously measuring the QCM resonant frequency and damping voltage (proportional to energy dissipation). This approach is similar to that of Krim and co-workers who use the QCM to measure the energy dissipation during condensation of rare gases onto the electrodes at cryogenic temperatures [20]. However our experiments differ in that the alkanethiol monolayer is strongly chemisorbed to the Au electrode surface in a corrugated potential that imposes specific adsorption sites. Therefore, the energy dissipation that we measure originates within the monolayer itself and is not due to monolayer "sliding" on the Au substrate.

In some experiments, an effusive molecular beam doser was used to enhance the effective pressure at the gold surface. Control experiments using rare gases, which do not adsorb on gold at 25°C, confirmed that ambient gas contributions to the energy dissipation are entirely negligible below 10^{-3} torr.

Identical procedures were used in an ultra-high vacuum surface analysis chamber equipped for simultaneous spectroscopic ellipsometry (SE) and QCM measurements. After obtaining reference optical spectra of the clean substrate, changes in the ellipsometric parameters Ψ and Δ were measured at 400 nm concurrently with the QCM data during monolayer growth. The Δ data were converted to *approximate* film thicknesses using a homogeneous film model and assuming that the monolayer film index of refraction is 1.49 at 400 nm. Reasonable variations in this index do not lead to significant changes in the resulting film thickness estimates. Although the QCM and other acoustic transducers have been used previously to study alkanethiol monolayers [22-24], these are the first to measure the energy dissipation, adsorption kinetics and optical thickness during the self-assembly process.

3. Results & Discussion:

Alkanethiol structural studies by others [3-11] have led to the self-assembly mechanism shown schematically in Figure 2. Here we explicitly distinguish among gas phase and physisorbed molecules (RS-H), chemisorbed monomers (RS) and chemisorbed dimers (RS-SR) in both fluid and solid states (where R = alkane chain) because each may contribute differently to the ensemble viscous properties. After an exposure of ~100L (1L = 10^{-6} torr sec), the adsorbed molecules condense into islands of the "striped" phase. STM data show that this phase consists of dimerized thiols (R-S-S-R) with co-linear alkane chains oriented parallel to the surface [8]. These dimers are arranged in stripes, analogous to the rungs of a ladder. As the exposure increases, the striped and c(4x2) solid phases co-exist until compression converts the striped domains into the c(4x2) structure. We note that the assembly process is not strictly sequential since multiple phases are known to co-exist at intermediate coverages.

Figure 3(a) shows representative data for C_9 thiol adsorption at 23.1°. The monotonic frequency decline (solid line, left scale) is proportional to the alkanethiol mass density on the electrode surface [25]. Since the ideal c(4x2) packing density is known, the frequency shift can be can be converted to the time-dependent coverage estimate shown by the solid line in Figure 3(b). Although this adsorption isotherm is suggestive of Langmuir adsorption kinetics, more detailed studies (see below) reveal important initial deviations indicative of precursor kinetics. The concurrently measured energy dissipation in Figure 3(a) (dashed line, right scale) initially increases sharply, maximizes in the coverage regime where striped and c(4x2) solid phases co-exist, and begins to decrease as the monolayer approaches saturation coverage. This behavior suggests that molecular motion at domain boundaries is an important contribution to monolayer dissipation.

Abruptly terminating the incident gas flux causes a drop in the dissipation and a slight gain in the frequency. These observations are readily understood as desorption of a physisorbed molecular state (R-S-H), in equilibrium with the gas phase. Evidence for such a physisorbed state has been reported previously [26, 27]. The rapid depletion of this state confirms that it is only weakly bonded to the SAM, and hence only weakly coupled to the moving QCM electrode. Although the physisorbed molecules contribute very little to the effective mass felt by the QCM, they do contribute significantly (~10 mV) to the overall dissipation.

The energy dissipation divided by the derived coverage is shown in Figure 3(b). This is analogous to an average viscosity of the adsorbed ensemble. The initial values are not shown since dividing a small dissipation by a small coverage leads to a large uncertainty. These data show that the average viscosity varies while striped and c(4x2) domains co-exist but drops by ~20% overall as the monolayer becomes more homogeneous. The viscous contribution by the weakly adsorbed physisorbed molecules is quite apparent when they are pumped off the surface. Thus the relative contributions to energy dissipation in the growing C_9 thiol monolayer by different structural features are: Physisorbed molecules >> mixed domain boundaries > c(4x2) domain boundaries

Interestingly, close inspection of the leading edge reveals that the energy dissipation increases slightly before the frequency begins to decline. This is investigated more carefully by thiol adsorption at 5×10^{-8} torr, shown in Figure 4. At this lower pressure, the equilibrium coverage of physisorbed molecules, and hence the magnitude of the measured dissipation, is reduced. Note the different behavior of the frequency change and dissipation with time. The *initial* C_9 thiol molecules contribute proportionately more to the dissipation than they do to the effective "mass loading;" i.e., they are adsorbed in a fluid phase that is only weakly coupled to the Au(111) substrate. However, the population of a fluid physisorbed state alone cannot account for the subsequent drop in dissipation (after ~38 min) followed by a gradual linear increase (at ~48 min) while the mass loading (coverage) monotonically increases. This behavior is suggestive of reaching a critical fluid coverage at which nucleation of the ordered stripe phase begins. Hence these fluid molecules must be chemisorbed (R-S). The dissipation climbs again as the mixed chemisorbed-fluid/solid-stripe phase grows. Returning to Figure 2, we now have direct evidence of not only the gas-physisorption equilibrium but also for the chemisorbed-fluid phase from which the strip phase is nucleated.

Simultaneous QCM and spectroscopic ellipsometry measurements of C_9 thiol adsorption, shown in figure 5, provide an optical signature of the monolayer growth. As before, the frequency change data are converted into the approximate coverage (Figure 5a). Assuming the simplest optical model, i.e. a homogeneous organic film, we see from figure 5(b) that the initial rapid adsorption leads to a film of ~3Å thickness, consistent with the alkanethiol hydrocarbon chains being oriented essentially parallel to the surface in the physisorbed, chemisorbed-fluid and solid striped phases. This independently confirms STM images that show near vertical chain orientations only as c(4x2) islands are formed at much higher coverages. This chain re-orientation is clearly seen in the SE data of figure 5(b) by the increasing optical (average) film thickness with time.

Finally, as we noted earlier, the adsorption kinetics cannot be well-fit by a Langmuir isotherm due to a nearly linear initial region where the sticking probability is independent of coverage. This implicates a precursor state mechanism, which is the subject of another publication [28]. Although the precursor mechanism dominates for longer chain alkanethiols [28], we can demonstrate that it is an operative adsorption channel for the C_9 thiol as well. In figure 6, adsorption at 5 x 10^{-7} torr clearly exhibits the initial linear region followed by a very gradual subsequent uptake. Increasing the ambient pressure by an order of magnitude accelerates the uptake. Whereas experiments conducted at effective pressures above 10^{-6} torr temporally compress these steps into a pseudo-Langmuir uptake curve, deviations are always evident in the initial coverage behavior.

Although a conclusive determination of the precursor cannot be made at this time, it is useful to consider the role of van der Waals interactions in the adsorption kinetics. Other work has provided evidence that the adsorbed thiols are dimerized not only in the striped phase but also in the c(4x2) phase [13, 29]. For a longer chain alkane thiol, the enhanced van der Waals interaction between adsorbed monomers and between a monomer and the gold substrate may increase its surface residence time and, therefore, its probability to dimerize. (Dimerization of the incident gas phase molecules is also a possibility.) Concerted dimerization may be a facile mechanism to dehydrogenate the physisorbed alkanethiol molecules, i.e., $\text{R-S-H} + \text{R-S-H} \Rightarrow \text{R-S-S-R} + \text{H}_2(g)$. If dimerization is an expeditious means to nucleate and stabilize the solid stripe phase, then this could be a critical kinetic step in the monolayer growth mechanism.

4. Conclusions:

Quartz crystal microbalance techniques and spectroscopic ellipsometry have been used to simultaneously measure the energy dissipation, adsorption kinetics and optical thickness during the self-assembly process for a C_9 thiol monolayer. Physisorbed molecules (R-S-H) in equilibrium with the ambient gas contribute ~20% of the overall measured viscous dissipation.

Domain boundaries in mixed fluid/solid phases are the second major contribution to energy loss in the growing monolayer. Evidence was found for a chemisorbed-fluid phase (R-S) from which the striped-solid phase is nucleated. Deviations from Langmuir adsorption kinetics show that a precursor–mediated adsorption channel is available for C_9 thiols.

These findings demonstrate that the intrinsic dissipative processes vary greatly with the phase and domain structure of the C_9 thiol monolayer and other alkanethiols as well [28]. Hence tribological measurements on differently prepared monolayers could likely yield disparate and "non-representative" results. Furthermore, the extension of single asperity friction results on a single domain to mesoscopic contact regions (e.g. MEMs) must be done with caution since energy dissipation at domain boundaries can dominate monolayer behavior.

Acknowledgements:

This work was supported by the DOE Office of Basic Energy Sciences, Division of Materials Sciences. Sandia is a multiprogram laboratory operated by Sandia Corporation, a Lockheed Martin Company, for the U.S. DOE under Contract DE-AC04-94AL85000.

References:

[1] A. Ulman, Chem. Rev. 96 (1996), 1533.

[2] H. I. Kim, T. Koini, T. R. Lee and S. S. Perry, Langmuir 13 (1997), 7192.

[3] L. H. Dubois and R. G. Nuzzo, Annu. Rev. Phys. Chem. 43 (1992), 437.

[4] E. Delamarche, B. Michel, H. A. Biebuyck and C. Gerber, Adv. Mater. 8 (1996), 719.

[5] G. E. Poirier, M. J. Tarlov and H. E. Rushmeir, Langmuir 10 (1994), 3383.

[6] N. Camillone III, P. Eisenberger, T. Y. B. Leung, P. Schwartz, G. Scoles, G. E. Poirier and M. J. Tarlov, J. Chem. Phys. 101 (1994), 11031.

[7] N. Camillone III, T. Y. B. Leung, P. Schwartz, P. Eisenberger and G. Scoles, Langmuir 12 (1996), 2737.

[8] G. E. Poirier and E. D. Pylant, Science 272 (1996), 1145.

[9] F. Schreiber, A. Eberhardt, T. Y. B. Leung, P. Schwartz, S. M. Wetterer, D. J. Lavrich, L. Berman, P. Fenter, P. Eisenberger and G. Scoles, Phys. Rev. B (in press).

[10] P. Fenter, Thin Films (in press).

[11] G. E. Poirier and M. J. Tarlov, Langmuir 10 (1994) 2853.

[12] Ch. Zubrägel, C. Deuper, F. Schneider, M. Neumann, M. Grunze, A. Schertel and Ch. Wöll, Chem. Phys. Lett. 238 (1995), 308.

[13] P. Fenter, A. Eberhardt and P. Eisenberger, Science 266 (1994), 1216.

[14] N. D. Shinn, R. Limary, C. Daly, T. A. Michalske and U. Landman, to be published.

[15] C. Lu and A. W. Czanderna, eds. *Applications of Piezoelectric Quartz Crystal Microbalances* (Elsevier, New York, 1984).

[16] C. D. Stockbridge, in *Vacuum Microbalance Techniques*, edited by K. H. Behrndt (Plenum, New York, 1966) Vol. 5, p. 193.

[17] S. J. Martin, V. E. Granstaff and G. C. Frye, Anal. Chem 63 (1991), 2272.

[18] R. Lučklum and P. Hauptmann, Faraday Discussions 107 (1997) 123.

[19] K. Wessendorf (patent pending).

[20] J. Krim and A. Widom, Phys. Rev. B38 (1988), 12184.

[21] H. G. Tompkins, *A User's Guide to Ellipsometry* (Academic Press, San Diego, 1993).

[22] D. S. Karpovich and G. J. Blanchard, Langmuir 10 (1994), 3315.

[23] Y. J. Lee, I. C. Jeon, W. Paik and K. Kim, Langmuir 12 (1996), 5830.

[24] R. C. Thomas, L. Sun, R. M. Crooks and A. J. Ricco, Langmuir 7 (1991), 620.

[25] Since the alkane thiol monolayer is viscoelastic, the "rigid mass" assumption commonly used to equate frequency shifts to adsorbed mass is rigorously invalid but an acceptable approximation.

[26] K. A. Peterlinz and R. Georgiadis, Langmuir 12 (1996), 4731.

[27] D. G. Castner, K. Hinds and D. W. Grainger, Langmuir 12 (1996), 5083.

[28] N. D. Shinn, T,. Mayer and T. A. Michalske, to be published.

[29] J. J. Gerdy and W. A. Goodard, III, J. Am. Chem. Soc. 118 (1996), 3233.

Figure Captions:

Figure 1: Schematic model of the c(4x2) solid phase of a linear alkanethiol monolayer on Au(111). The equilibrium polar tilt angle is ~34°. Three tilted domains are possible due to the c_{3v} azimuthal symmetry of the Au(111) substrate.

Figure 2: Schematic representation of the self-assembly process distinguishing physisorbed (R-S-H) and chemisorbed (R-S) phases.

Figure 3: (a) Measured QCM frequency change (solid line) and energy dissipation (open circles) during C_9 thiol monolayer growth for doser-enhanced exposure. The ambient background pressure was ~ 5×10^{-6} torr. Note changes upon evacuation of ambient thiol gas. (b) Alkanethiol coverage (solid line) and average dissipation per unit coverage (solid squares) as a function of time for the data in panel (a).

Figure 4: Measured QCM frequency change (solid line) and energy dissipation (open circles) during the initial C_9 thiol adsorption at ~5×10^{-8} torr.

Figure 5: Simultaneous QCM and spectroscopic ellipsometry data for C_9 thiol adsorption at 1×10^{-6} torr: (a) QCM frequency change; (b) Ellipsometric parameter delta measured at $h\nu = 400$ nm.

Figure 6: Measured QCM frequency change during C_9 thiol adsorption at 5×10^{-7} torr and following a subsequent pressure increase to 5×10^{-6} torr. Initial linear slope indicates precursor mediated adsorption kinetics.

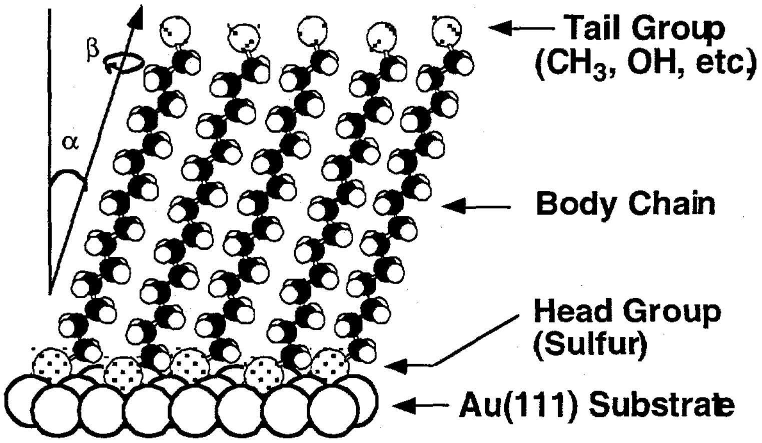

Figure 1

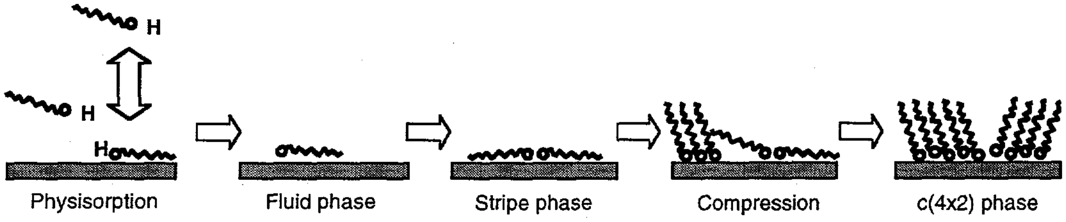

Figure 2

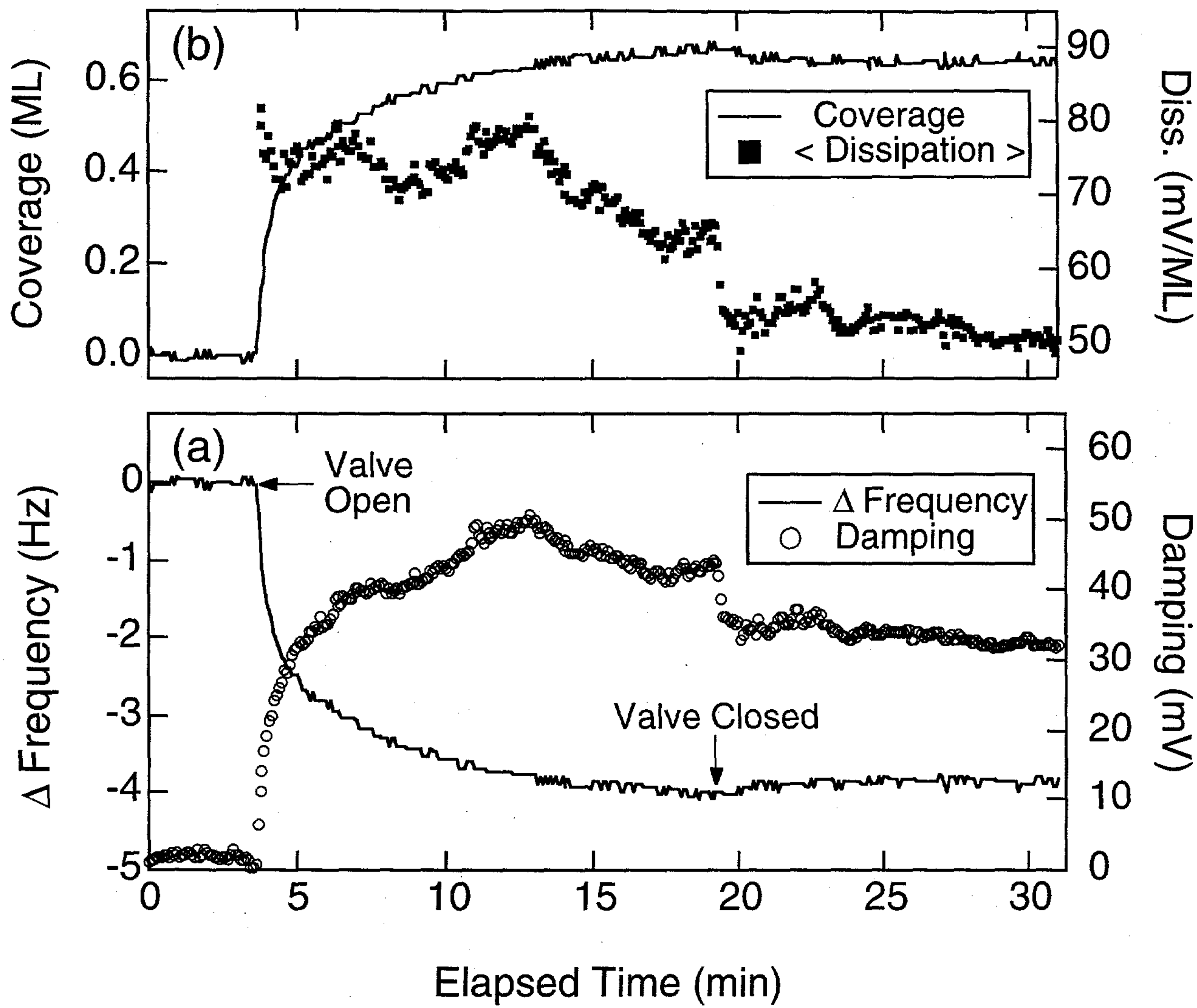
(b)
Coverage (ML)
0.0
0.2
0.4
0.6
Diss. (mV/ML)
50
60
70
80
90
Coverage
■ < Dissipation >
(a)
Valve Open
Valve Closed
Δ Frequency (Hz)
0
-1
-2
-3
-4
-5
Damping (mV)
0
10
20
30
40
50
60
Δ Frequency
○ Damping
0
5
10
15
20
25
30
Elapsed Time (min)

Figure 3

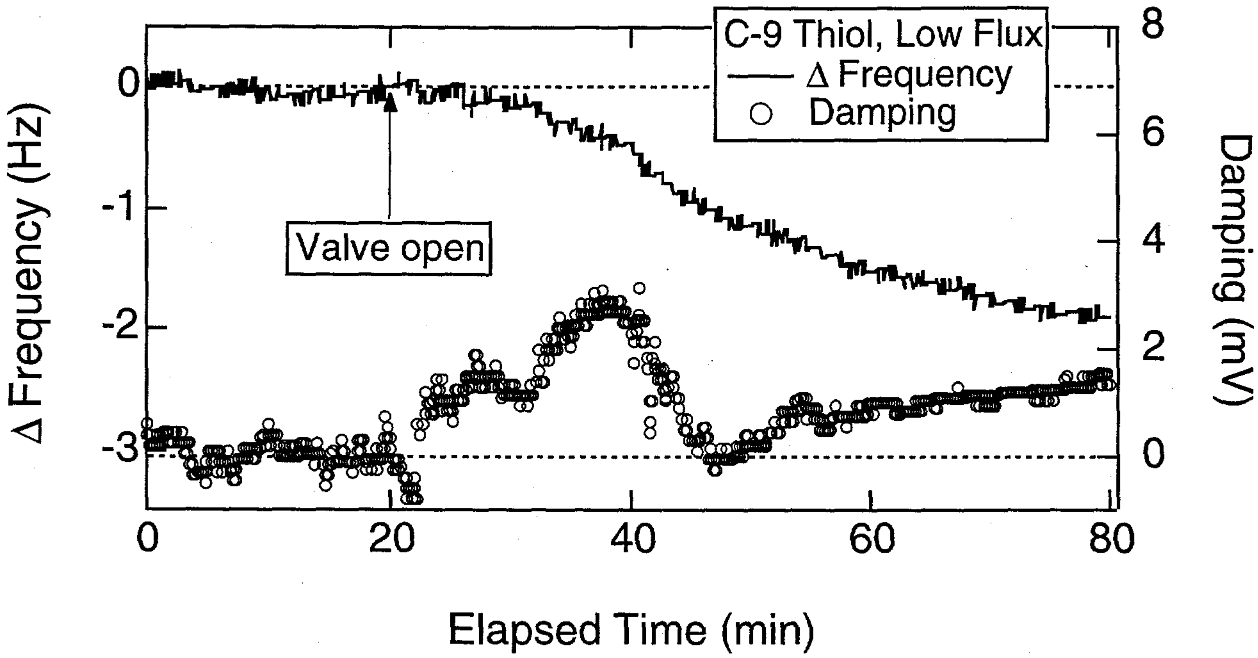
C-9 Thiol, Low Flux
Δ Frequency
Damping
Valve open
Δ Frequency (Hz)
0
-1
-2
-3
Damping (mV)
8
6
4
2
0
Elapsed Time (min)
0
20
40
60
80

Figure 4

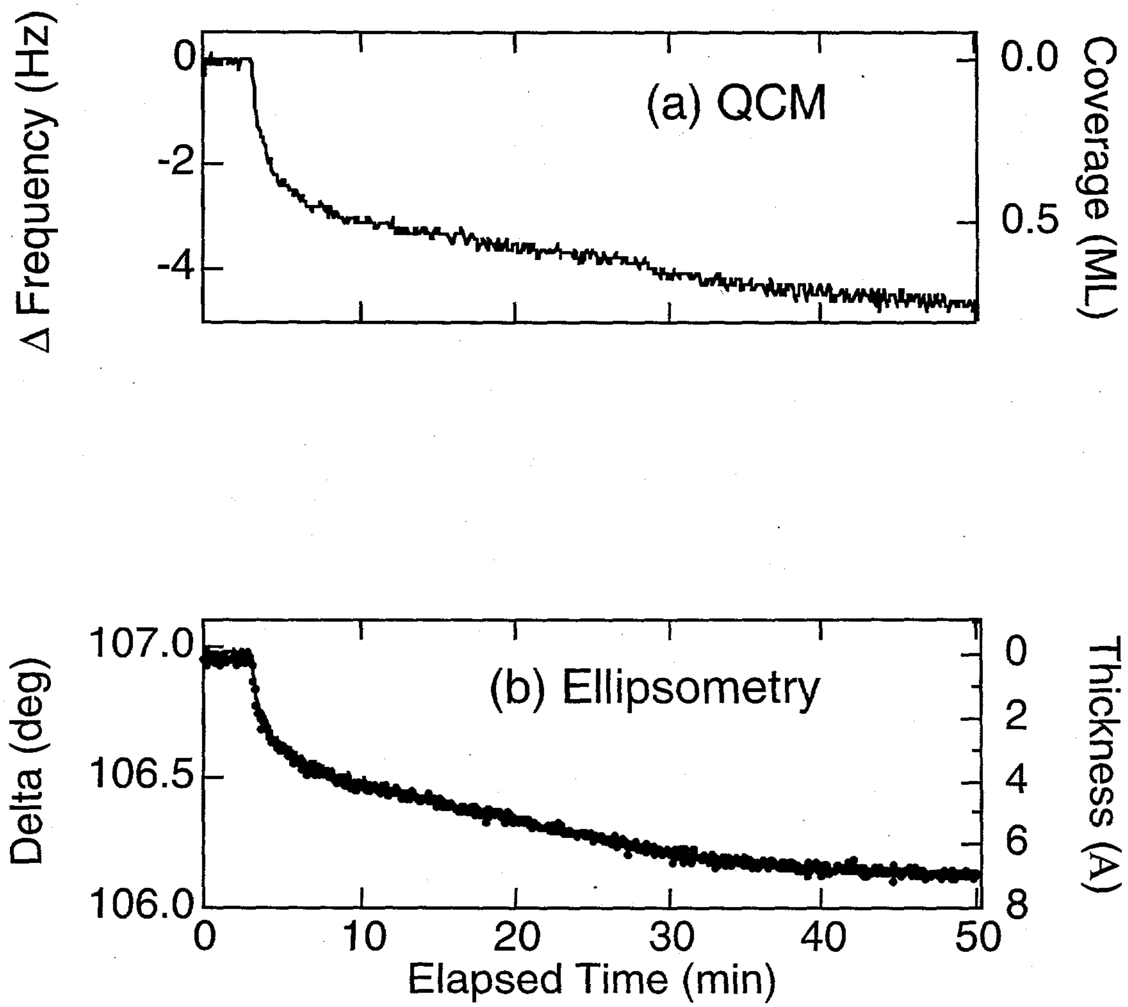
(a) QCM
Δ Frequency (Hz)
0
-2
-4
Coverage (ML)
0.0
0.5
(b) Ellipsometry
Delta (deg)
107.0
106.5
106.0
Thickness (A)
0
2
4
6
8
0
10
20
30
40
50
Elapsed Time (min)

Figure 5

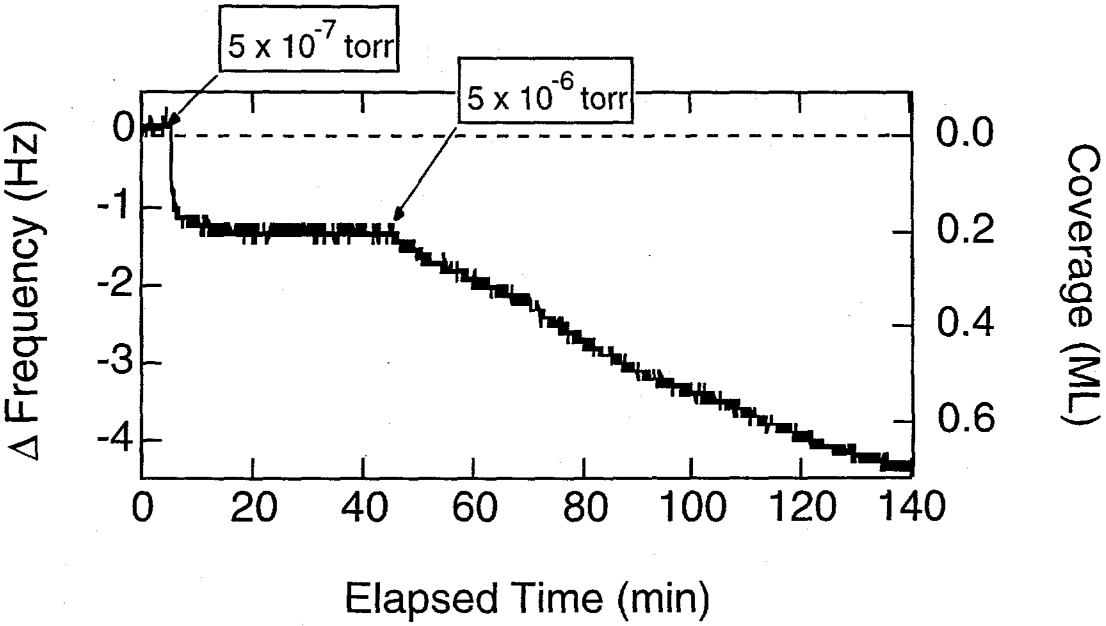
5 x 10^{-7} torr
5 x 10^{-6} torr
Δ Frequency (Hz)
0
-1
-2
-3
-4
Coverage (ML)
0.0
0.2
0.4
0.6
Elapsed Time (min)
0
20
40
60
80
100
120
140

Figure 6